Murine models of sickle cell disease and beta-thalassemia demonstrate pulmonary hypertension with distinctive features

Paul W. Buehler[1,2] , **Delaney Swindle**[3], **David I. Pak**[3], **Mehdi A. Fini**[3], **Kathryn Hassell**[4], **Rachelle Nuss**[4], **Rebecca B. Wilkerson**[5], **Angelo D'Alessandro**[5] and **David C. Irwin**[3]

[1]Department of Pathology, University of Maryland School of Medicine, Baltimore, MD, USA; [2]The Center for Blood Oxygen Transport, Department of Pediatrics, University of Maryland School of Medicine, Baltimore, MD, USA; [3]Cardiovascular and Pulmonary Research Laboratory, Department of Medicine, University of Colorado Denver – Anschutz Medical Campus, Aurora, CO, USA; [4]Division of Hematology Colorado Sickle Cell Treatment and Research Center, School of Medicine, Anschutz Medical Campus, University of Colorado-Denver School of Medicine, Aurora, CO, USA; [5]Department of Biochemistry and Molecular Genetics, University of Colorado Denver – Anschutz Medical Campus, Aurora, CO, USA

Abstract

Sickle cell anemia and β-thalassemia intermedia are very different genetically determined hemoglobinopathies predisposing to pulmonary hypertension. The etiologies responsible for the associated development of pulmonary hypertension in both diseases are multi-factorial with extensive mechanistic contributors described. Both sickle cell anemia and β-thalassemia intermedia present with intra and extravascular hemolysis. And because sickle cell anemia and β-thalassemia intermedia share features of extravascular hemolysis, macrophage iron excess and anemia we sought to characterize the common features of the pulmonary hypertension phenotype, cardiac mechanics, and function as well as lung and right ventricular metabolism. Within the concept of iron, we have defined a unique pulmonary vascular iron accumulation in lungs of sickle cell anemia pulmonary hypertension patients at autopsy. This observation is unlike findings in idiopathic or other forms of pulmonary arterial hypertension. In this study, we hypothesized that a common pathophysiology would characterize the pulmonary hypertension phenotype in sickle cell anemia and β-thalassemia intermedia murine models. However, unlike sickle cell anemia, β-thalassemia is also a disease of dyserythropoiesis, with increased iron absorption and cellular iron extrusion. This process is mediated by high erythroferrone and low hepcidin levels as well as dysregulated iron transport due transferrin saturation, so there may be differences as well. Herein we describe common and divergent features of pulmonary hypertension in aged Berk-ss (sickle cell anemia) and Hbb$^{th/3+}$ (intermediate β-thalassemia) mice and suggest translational utility as proof-of-concept models to study pulmonary hypertension therapeutics specific to genetic anemias.

Introduction

Sickle cell anemia (SCA) and β-thalassemia are genetically determined hemoglobinopathies and affect millions of people globally. SCA is caused by a single point mutation (Glu6Val) in the beta-globin gene and results in the synthesis of abnormal hemoglobin (Hb-S) that generates long strand Hb-S polymers and the characteristic sickling of red blood cells (RBCs) in those homozygous for the mutation.[1,2] RBC injury and subsequently erythrophagocytosis leads iron accumulation in monocytes/macrophages, heme loss and partitioning as well as extracellular hemoglobin.[3,4]

On the other hand, β-thalassemia is associated with dyserythropoiesis and a broad range of disease severity (i.e. thalassemia minor, intermedia and major) that are defined by

Corresponding authors:
Paul W. Buehler, Department of Pathology University of Maryland School of Medicine, HSF III, 8th Floor, Room 8180, Baltimore, MD 21201, USA.
Email: pbuehler@som.umaryland.edu
David C. Irwin, Department of Cardiology, University of Colorado Anschutz, Medical Campus Research Building 2, B133, Room 8121 Aurora, Colorado 80045, USA.
Email: david.irwin@cuanschutz.edu

numerous documented Hbb gene mutations.[5,6] The cause of disease is an imbalance in normal β/γ-globin chain relative to α-globin chain synthesis leading to intracellular α-globin chain accumulation in the absence of α-hemoglobin stabilizing protein.[5,7] Free intracellular α-globin is prone to oxidation, heme disorientation and pro-oxidative hemichromes that injure the RBC.[8] Extravascular hemolysis and export of iron from macrophages and hepatocytes[9] is a significant contributor to excess iron in patients with β-thalassemia, along with paradoxical iron absorption from the gut,[9] and ultimately iron loading from intermittent or repeated transfusions.[5]

A shared potential comorbidity of SCA and β-thalassemia is pulmonary hypertension (PH) with right ventricular dysfunction. The prevalence of PH is 6–10% of the SCA patient population based on cardiac catheterization.[10–12] The risks for development of SCA-PH are defined and heavily weighted toward the frequency and extent of hemolysis and nitric oxide consumption,[13] hypercoagulability,[14] increasing age,[15] renal dysfunction[16] and transfusion-dependent iron overload.[17,18] In comparison and based on cardiac catheterization, the prevalence of PH concomitant with β-thalassemia is estimated to be 4.8% and 2.1% for β-thalassemia intermedia and major, respectively. The most critical risk factors for the onset of PH in both intermediate and major forms of disease are aging and whether a splenectomy has occurred.[5,19] In addition, following splenectomy, intermediate β-thalassemia and E/β-thalassemia patients demonstrate intravascular hemolysis[20,21] and RBC microparticle-induced endothelial dysfunction with thrombosis[22] in association with PH development. All forms of PH, including SCA and β-thalassemia, are associated with dramatic structural remodeling of the pulmonary vasculature,[23] elevated PA pressures (>25 mmHg), right ventricular hypertrophy, and cardiac dysfunction. Thus, the symptomatology and outcomes are primarily determined by right ventricular failure caused by increased PA pressures.

Transgenic murine models of SCA (Berk-ss) expressing human α and β^S globin[24–26] exhibit multi-organ pathologies that manifest spontaneously and include hemolysis resulting in severe anemia, iron accumulation (splenic, hepatic, renal, and pulmonary) and cardiopulmonary abnormalities that approximate homozygous disease in humans.[24–26] Deletion of both β^{minor} and β^{major} genes on one beta globin allele and the other normal define the β-thalassemia intermedia mice (Hbb$^{th3/+}$) that demonstrate mild anemia, splenomegaly, and iron accumulation in all organs.[7,27] We report extensive iron-loaded macrophages in remodeled human SCA-PH pulmonary vascular tissue and in rodent models of SCA-PH.[4] Commonalities in SCA macrophage iron accumulation and iron overload in β-thalassemia suggests a potential anemia independent contribution to PH that warrants study. The evaluation of transgenic murine models is necessary to further a mechanistic understanding of cardiopulmonary disease in these common hemoglobinopathies. Nonetheless, an a priori comparison of PH and cardiac function in Berk-ss and Hbb$^{th3/+}$ has not been performed. In the current study, we hypothesized that both Berk-ss and Hbb$^{th3/+}$ mice develop pulmonary vascular remodeling, PH and right ventricular dysfunction, similarly. To this end, studies were undertaken to assess cardiopulmonary dysfunction and determine lung and right ventricular metabolism in age and sexed match Berk-ss and Hbb$^{th3/+}$ mice.

Materials and methods

Ethical approval and animal care

Young-adult male and female C57Bl/6 WT and Berk-ss mice (eight weeks old) were obtained from Jackson Laboratories (Bar Harbor, ME, USA) and Hbb$^{th3/+}$ (eight weeks old) were obtained from Dr. Jaro Vostal, MD, PhD (FDA, Center for Biologics Evaluation and Research, Silver Spring, MD, USA) to establish breeding colonies. A total of 77 mice (WT: n = 15, Hbb$^{th3/+}$: n = 24 and Berk-ss: n = 38) were evaluated at 20–28 months of age. All experimental procedures were conducted under the guidelines recommended by *The Journal of Physiology*[28] and were approved by the Institutional Animal Care and Use Committee at the University of Colorado, Denver, Anschutz Medical Campus.

Open chest solid state catheterization for right ventricular function analysis

Aged mice underwent terminal open chest right ventricular (RV) function measurements with a 1.2F, FTE-1212B-4018 pressure volume catheter (Transonic Systems Inc., Ithaca, NY) inserted by direct cardiac puncture. Anesthesia induction was achieved with inhaled isoflurane (4–5%), and a tracheal incision (∼1 cm) was performed. Next, a tracheal tube was inserted and connected to an Anesthesia Workstation or Hallowell EMC Microvent and a plane was maintained at 1.0–2.5% isoflurane in 100% oxygen. Then, a thoracotomy was performed exposing the heart, the pericardium was resected and a small hole made at the base of the RV with a 30 g needle for insertion of the pressure–volume catheter. Steady-state hemodynamics are collected with short pauses in ventilation (up to 10 s) or high-frequency oscillatory ventilation to eliminate ventilator artifact from the pressure–volume recordings. Occlusions of the inferior vena cava were performed by applying pressure to the inferior vena cava (up to 10 s) through the abdominal opening. After the pressure–volume and hemodynamic measurements completed, mice were humanely euthanized by exsanguination and cervical dislocation. Data were recorded continuously using LabScribe2 and analyzed offline.

Blood and organ collection

At the end of the experimental protocol, 0.8 mL of blood was collected and placed in an EDTA-K+ vacutainer and a hematocrit (Hct) tube for analysis of Hct and archiving of plasma. Tissues were collected after PBS perfusion as reported previously.[29] The hearts were removed, and the RV and left ventricle (LV) with septum (LV + S) were weighed for the assessment of the Fulton Index (RV/LV + S). RV and half of the lung were snap frozen for metabolomic analysis. The other half of the lung was perfused and inflated, fixed in formalin for 24 h, and stored in 85% ethanol prior to paraffin embedding and tissue sectioning.

Histology and morphology

Tissue sections were dewaxed and rehydrated and processed as previously described.[29] Five-micron lung sections were stained with hematoxylin and eosin (H&E) by standard procedures to assess the accumulation of perivascular cells as well as vessel wall thickness as previously described.[30] Briefly, lung vascular remodeling was quantified for the H&E stained lung tissue sections. Scanned images were equally divided into 100 equal segments. Images that did not have sufficient vessels in the segment were excluded and from the remaining images, 10 randomly selected segments were used for analysis. Using the program STEPanizer (Tschanz & Weibel, 2011), a grid was overlaid on each image and was used to quantify the vasculature within each image. The percentage of vascular tissue to parenchymal tissue in the lung was calculated.

Perls iron staining was performed on tissue sections incubated with Perls iron reagent containing 5% potassium ferrocyanide and 2% hydrochloric acid for 45 min at room temperature and rinsed in deionized water. Sections were then incubated with 0.3% hydrogen peroxide and 0.01 M sodium azide in methanol for 30 min at room temperature. All sections were then rinsed in 0.1 M phosphate buffer, pH 7.4, incubated with DAB (SigmaFast DAB, Sigma) for 3 min, washed in deionized water, and lightly counterstained with Gill's II hematoxylin.

Metabolomics

Lung and RV tissue homogenates (10 mg of tissue) were extracted in methanol: acetonitrile: water (5:3:2 v/v/v – at a 10 mg/ml ratio) prior to UHPLC-MS analyses (Vanquish-QExactive, Thermo Fisher), as described previously in the study of metabolic reprogramming in pulmonary hypertension,[31] with a focus on organ metabolism (including lungs[32] and RV[33]) and related technical notes.[34]

Statistical analysis

Data are presented as a mean ± standard error of the mean (SEM). Statistical comparisons for data measurements were completed with the analysis of variance (ANOVA) and *Post-hoc* analyses were completed with the Tukey-Kramer multiple comparison tests. Other non-parametric ANOVA (Kruskal Wallis with Dunns post-hoc) was used for metabolomics analyses. Strain effects between WT type and either $Hbb^{th3/+}$ or Berk-ss were completed using a Student's t-test. For metabolomics analyses, principal component analyses (PCA) and hierarchical clustering analyses were performed with the software MetaboAnalyst 5.0.[35] Statistical analysis was completed using the statistical software package GraphPad (version 9.1). Statistical significance was defined as $P \leq 0.05$.

Results

Assessment of pulmonary hypertension

To begin comparing basal pulmonary vascular phenotypes between aging WT, $Hbb^{th3/+}$, and Berk-ss mice, RV functional analysis was compared across the three genotypes of mice by analyzing pressure–volume (PV) loops with occlusion obtained from mice in each group. Compared to WT mice, both $Hbb^{th3/+}$ and Berk-ss mice have elevated RV systolic pressures (Pes; describing PA pressures; $\sim 23 \pm 1$ mm Hg vs. $\sim 32 \pm 1$ mm Hg; $p < 0.01$ vs. WT) (Fig. 1a), increased medial thickening ($p = <0.05$; vs. WT) (Fig. 1b), greater RV weights ($\sim 0.03 \pm 0.002$ g vs. $\sim 0.05 \pm 0.002$ g; $p < 0.013$ vs. WT) (Fig. 1c), and RV/BW ratios ($\sim 0.94 \pm 0.06$ vs. 1.6 ± 0.06 and 1.9 ± 0.08; WT, $Hbb^{th3/+}$ and Berk-ss, respectively; $p < 0.01$ vs. WT) (Fig. 1d). Despite the larger LV + S ratios observed in both $Hbb^{th3/+}$ and Berk-ss mice vs. WT cohorts (Fig. 1e), analysis of the Fulton index revealed that Berk-ss mice had a greater RV/LV + S ratios compared to WT and $Hbb^{th3/+}$ (0.35 ± 0.01 vs. $\sim 0.3 \pm 0.01$; $p < 0.05$ vs. WT and $Hbb^{th3/+}$) (Fig. 1f). Analyses for sex differences within strains show no differences (data not shown). Taken together, these data demonstrate that unlike WT as both male and female $Hbb^{th3/+}$ and Berk-ss transgenic mice naturally develop PH and RV hypertrophy.

Based on our reported observations in human SCA PH that demonstrate pulmonary vascular iron macrophage accumulation[4] and the results presented in Fig. 1, we next stained lung tissue to assess for pulmonary vascular iron accumulation. Lung tissue sections stained with Perls DAB are shown (Fig. 1g). Both $Hbb^{th3/+}$ and Berk-ss lung tissue sections reveal vessels with iron positive cells, suggesting a common feature associated with iron accumulated cells in the development of PH in the models.

Assessment of right ventricular function

Right ventricular hypertrophy and dysfunction is a hallmark of pulmonary vascular disease. Because $Hbb^{th3/+}$ and Berk-ss mice develop PH (as evidenced by elevated PA pressures and RV weights) with age, we sought to characterize and compare basal RV function across these
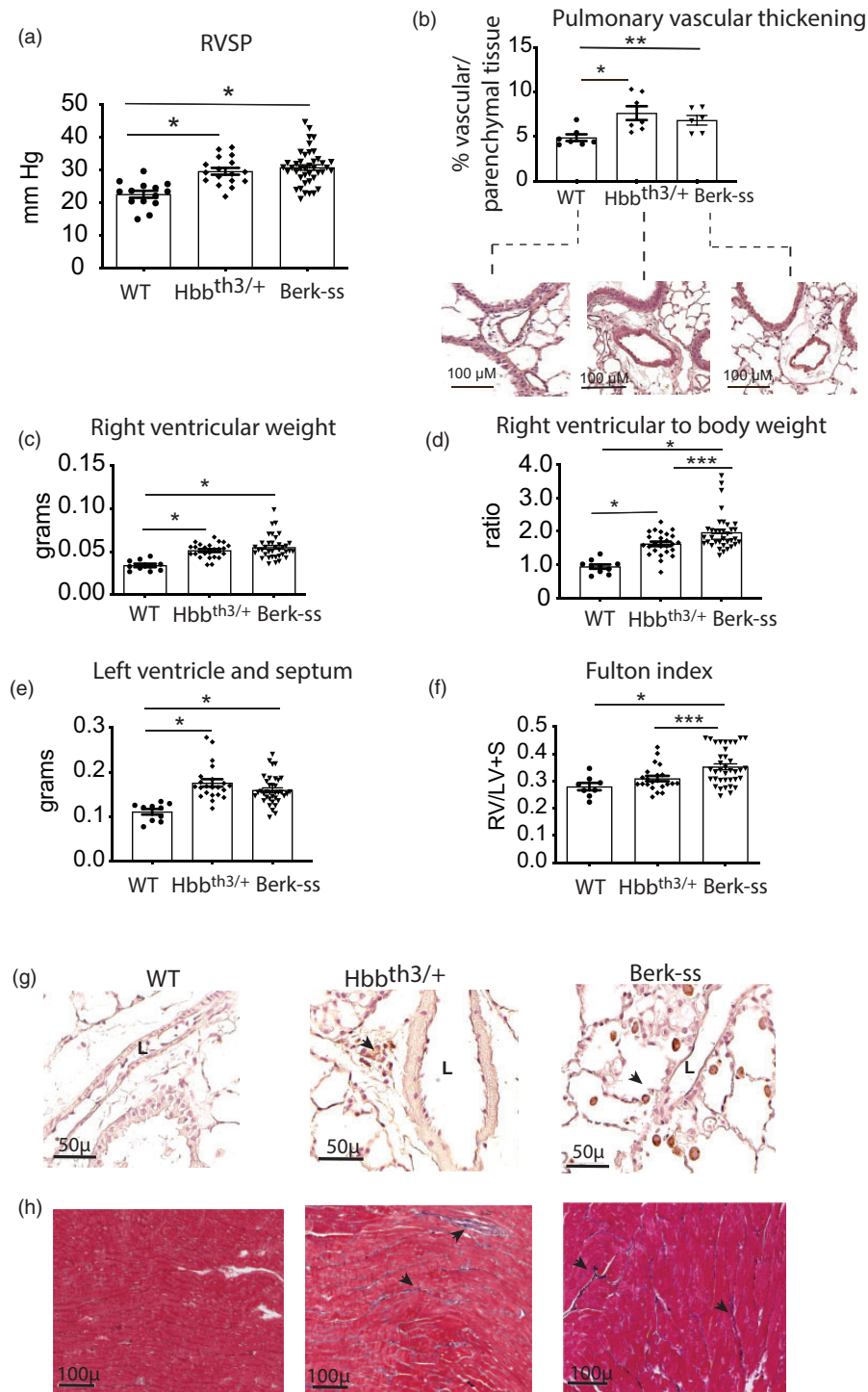
Fig. 1. Berk-ss and Hbb[th/3+] mice develop pulmonary hypertension with remodeling: (a) Right ventricular systolic pressures. (b) Pulmonary vascular remodeling. (c) right ventricular weight. (d) Right ventricular to body weight ratio. (e) Left ventricle plus septum weight. (f) Fulton index (RV/LV+S). (g) Iron loaded cells accumulate in the lungs of Berk-ss and Hbb[th3/+] mice. *p < 0.01 vs. wild type; **p < 0.05 vs. wild type t-test; ***p = 0.013 vs. Hbb[th3/+]. L: vessel lumen; black arrows showing iron-loaded cells. (h) Mild RV interstitial fibrosis following Masson's trichrome staining.

genotypes. Evaluation of PV loops with occlusions provides knowledge on: (1) intrinsic mechanical properties of the ventricle, (a) stiffness (end diastolic pressure volume relationship (EDPVR) and (b) elastance a measure of contractility (Ees); (2) the mechanical resistance forces on the RV and it's efficiency at ejecting blood into the PA, (a) afterload (Ea) and (b) energy transfer between ventricular contractility and arterial afterload as described by the
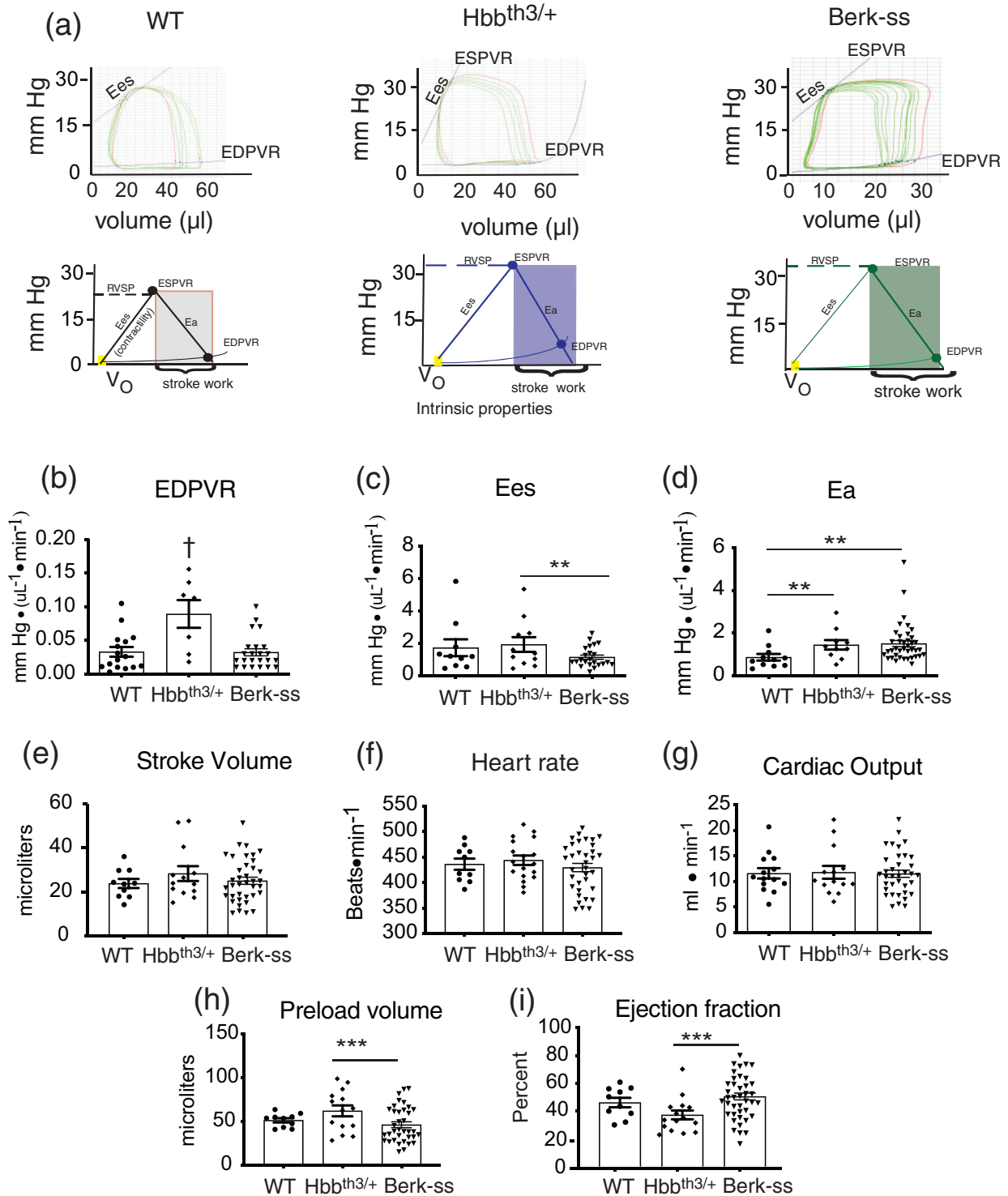
Fig. 2. Berk-ss and Hbb[th/3+] mice develop right ventricular mechanical dysfunction: (a) Representative tracings and corresponding schematics of pressure volume (PV) loop relationships during an occlusion for wild type, Hbb[th3/+], and Berk-ss mice. (b–j) Right ventricular functional analysis for stiffness, contractility, afterload, stroke volume, heart rate, cardiac output, right ventricle to pulmonary vascular coupling ratio, preload volume, and ejection fraction. *$p < 0.01$ vs. wild type; **$p < 0.05$ vs. wild type t-test; †$p < 0.01$ vs. Hbb[th3/+].

ventricular to vascular coupling ratio (VVCR); (3) the functional performance metrics of the ventricle, (a) cardiac output (CO), (b) stroke volume (SV), (c) heart rate, (HR), (d) preload volume, and (e) ejection fraction (see Fig. 2a).

Intrinsic mechanical properties: Pulmonary vascular disease in aging Hbb[th3/+] mice is associated with greater RV stiffness as evidenced by the higher EDPVR (Fig. 2b) values when compared to both WT and Berk-ss mice ($\sim 0.09 \pm 0.02$

vs. $\sim 0.03 \pm 0.005$ Hbb$^{th3/+}$ vs. WT and Berk-ss r; $p < 0.001$). In contrast, Hbb$^{th3/+}$ mice demonstrated comparable contractility (Ees) (Fig. 2c) to WT mice ($\sim 1.9 \pm 0.4$ vs. $\sim 1.7 \pm 0.5$), while contractility was significantly decreased in Berk-ss mice (1.1 ± 0.; $p = 0.04$ vs. Hbb$^{th3/+}$) (Fig. 2c). Further, both Hbb$^{th3/+}$ and Berk-ss mice demonstrate an increased RV afterload (Ea) (Fig. 2d), supportive of increased PA pressures in the two models. Taken together, these data suggest that Hbb$^{th3/+}$ mice have a restrictive physiology phenotype with preserved contractility, while aged Berk-ss mice demonstrate impaired RV contraction (Fig. 2b and c).

Right ventricular functional properties: To assess if changes in stiffness and contractility translated to changes in RV function, we compared stoke volumes (SV), cardiac output (CO), and heart rate (HR) in WT, Hbb$^{th3/+}$, and Berk-ss mice. Comparisons revealed no significant differences between SV, HR, or CO between the cohorts (Fig. 2e–g), but we did observe a lower preload volume in Berk-ss mice ($\sim 45 \pm 3.3\,\mu l$ vs. $\sim 58 \pm 6.2\,\mu l$ vs. Hbb$^{th3/+}$; $p = 0.013$) (Fig. 2h), which was compensated for by higher ejection fraction in Berk-ss mice ($50 \pm 2\%$ Berk-ss vs. $37 \pm 3\%$ vs. Hbb$^{th3/+}$; $p = 0.009$) (Fig. 2i). RV afterload was increase in Hbb$^{th3/+}$ and Berk-ss mice (Fig. 2h) demonstrating increased pulmonary vascular resistance, congruent with increased RV systolic pressures (Esp). Despite the increased RV afterload in Hbb$^{th3/+}$ and Berk-ss mice, the RV to pulmonary vascular coupling ratios remained consistent with WT demonstrating RV efficiency was preserved (Fig. 2j). These data demonstrate that the intrinsic mechanical properties of the RV in Hbb$^{th3/+}$ and Berk-ss mice develop differently, but do not lead to decompensated RV function with age.

Assessment of body weight, hematocrit, and splenomegaly

Berk-ss mice demonstrated the lowest body weights (28 ± 0.7 g vs. 38 ± 2.3 (WT) and 31 ± 1 (Hbb$^{th3/+}$); $p < 0.01$), greatest spleen weights (1.042 g ± 0.04 vs. 0.095 g ± 0.004 (WT) and 0.607 ± 0.07 (Hbb$^{th3/+}$); $p < 0.0001$), and Hct

(16 ± 0.6 vs. 42 ± 1 (WT) and 24 ± 1 (Hbb$^{th3/+}$); $p < 0.001$), whereas the Hbb$^{th3/+}$ mice demonstrated an intermediate phenotype (Fig. 3c and d). Congruent with the differences Hct and extra-medullary ineffective erythropoiesis, spleen weights were greatest in Berk-ss mice.

Metabolomics analysis

To better understand the differential underpinnings of PH in Hbb$^{th3/+}$ and Berk-ss mice the metabolism in lung and RV tissue were evaluated. Lung metabolic reprogramming is a hallmark of PH[36] and to date studies have focused on the specific metabolic adaptations of different cell types (e.g., fibroblasts,[37,38] macrophages,[39] and smooth muscle cells[40]) in the pulmonary vasculature that participate in the proliferation of the pulmonary adventitia and fibrosis. While results from evaluation of the RV are reported on in rodent PH models of SU5416-hypoxia-normoxia exposure,[33] limited information is available as to whether such metabolic adaptations are observed in the lungs and RV of murine models of hemoglobinopathies linked to PH. To bridge this gap, we performed metabolomics analyses of lung and RV tissues from WT, Hbb$^{th3/+}$, and Berk-ss mice. Results are reported more extensively in **Supplementary Table 1**. Unsupervised analyses were performed, including principal component analysis (PCA – Fig. 4a and b) and hierarchical clustering analysis of the most significant 25 metabolites by ANOVA across the three groups (Fig. 4c and d). Results suggest distinct metabolic signatures across the three groups in both tissues, with Berk-ss mice showing greater metabolic divergence from WT than the Hbb$^{th3/+}$ mice (Fig. 4a and b). Specifically, lungs from Berk-ss mice were characterized by a significant dysregulation of amino acid levels (methionine, leucine, phenylalanine, glutamine, aspartate) and decreased levels of several short and medium chain acyl-carnitines (C2, C8, C14) compared to WT and Hbb$^{th3/+}$ mice (Fig. 5a and b). Interestingly, decreases in glutamine and reduced glutathione were observed in lung tissue from Hbb$^{th3/+}$ mice, while Berk-ss lung tissue was characterized by increases in methionine – a scavenger of reactive oxygen
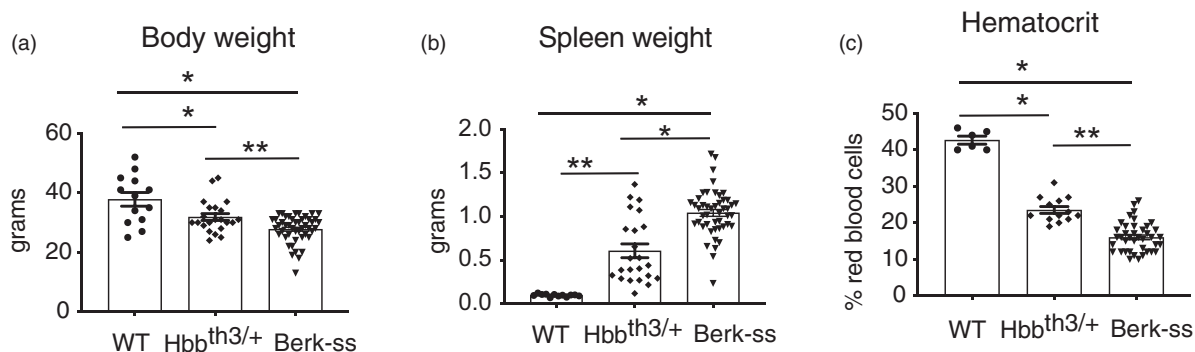

Fig. 3. Hbb$^{th3/+}$ mice develop an intermediate anemic phenotype: (a) body weight, (b) spleen weight, and (c) hematocrit. $*p < 0.007$ vs. wild type; $**p < 0.013$ vs. Hbb$^{th3/+}$.
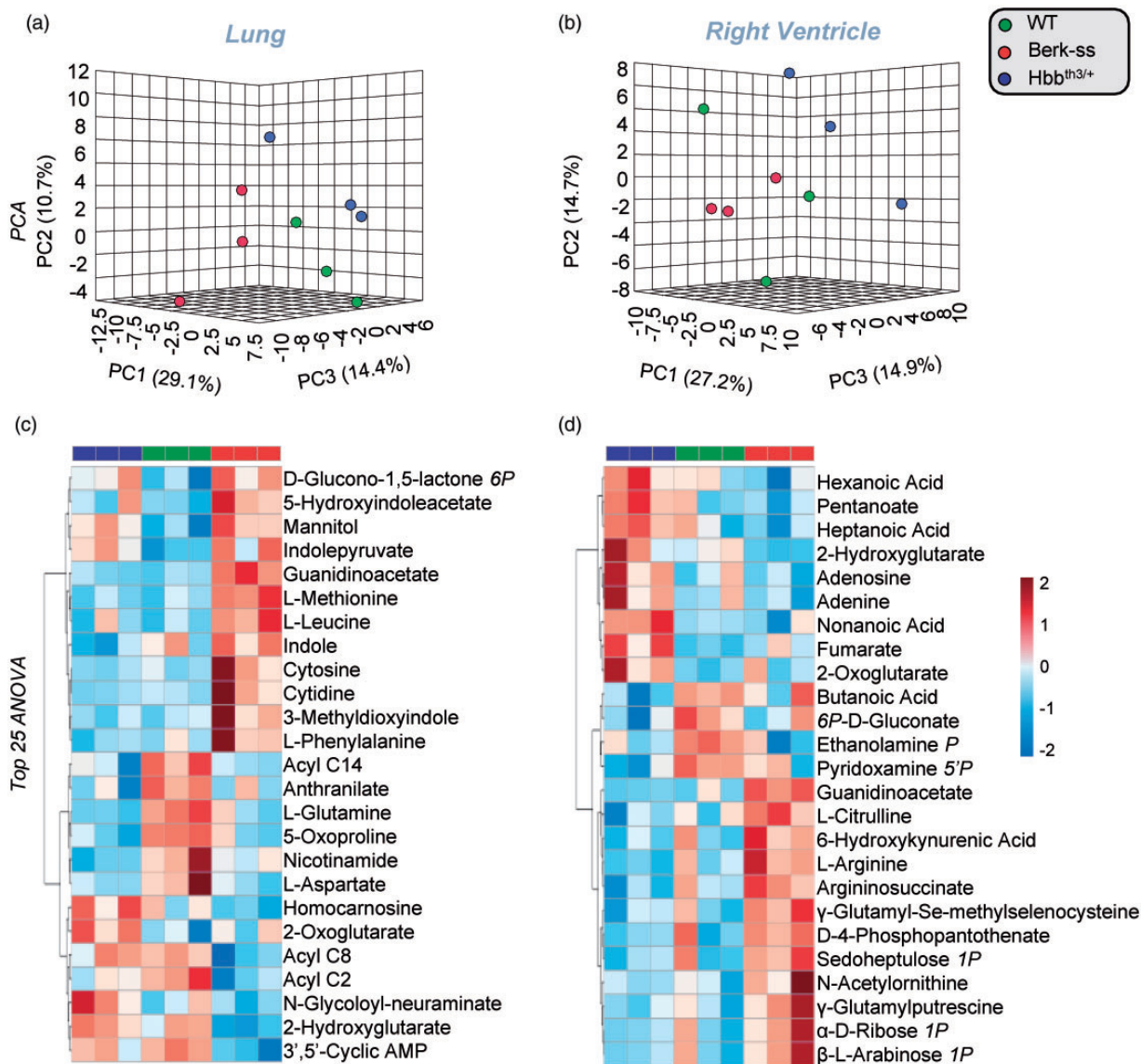
Fig. 4. Berk-ss and Hbb[th/3+] mice demonstrate unique lung and right ventricular metabolism across the 25 most significantly changed metabolites: Multivariate analyses of metabolomics data of lungs and right ventricle (RV) of wild type (WT – green), sickle cell disease (SCA – red) and beta-thalassemia mice (blue). Analyses included principal component analysis (PCA) in (a) and (b), and hierarchical clustering analyses of the top significant 25 metabolites by ANOVA (c and d).

species and contributor to the repair of reactive oxygen species-induced protein isoaspartyl damage (Fig. 5b). Altered carboxylic acid metabolism, with increases in 2-oxoglutarate and fumarate, decreased 2-hydroxyglutarate and significant accumulation of malate were noted in Berk-ss lung tissues (Fig. 5b). On the other hand, Hbb[th3/+] RV were characterized by higher levels of free short chain fatty acids (pentanoate, hexanoate, heptanoate, nonanoate) and carboxylic acids (2-oxoglutarate, fumarate), suggestive of altered lipid catabolism in mitochondria (Fig. 6a and b). RV from Berk-ss were characterized by higher levels of metabolites from the pentose phosphate pathway (phosphogluconate, ribose phosphate, sedoheptulose phosphate) (Fig. 6b), a pathway whose activation has been implicated

in the etiology of proliferative events in PH in other rodent models.[41] Increases in the levels of arginine, argininousccinate, citrulline, and guanidinoacetate – but not ornithine – in the RV of Berk-ss mice (Fig. 6a and b) is compatible with up-regulation of nitrogen metabolism through the urea cycle and/or the dysregulation of vasodilatory signaling through activation of nitric oxide synthase.

Discussion

Hemoglobinopathies associated with hemolysis, including β-thalassemia and SCA are associated with an increased incidence of PH.[42] The etiologies of PH in the disorders are increasing age and past splenectomy[35] as well as the
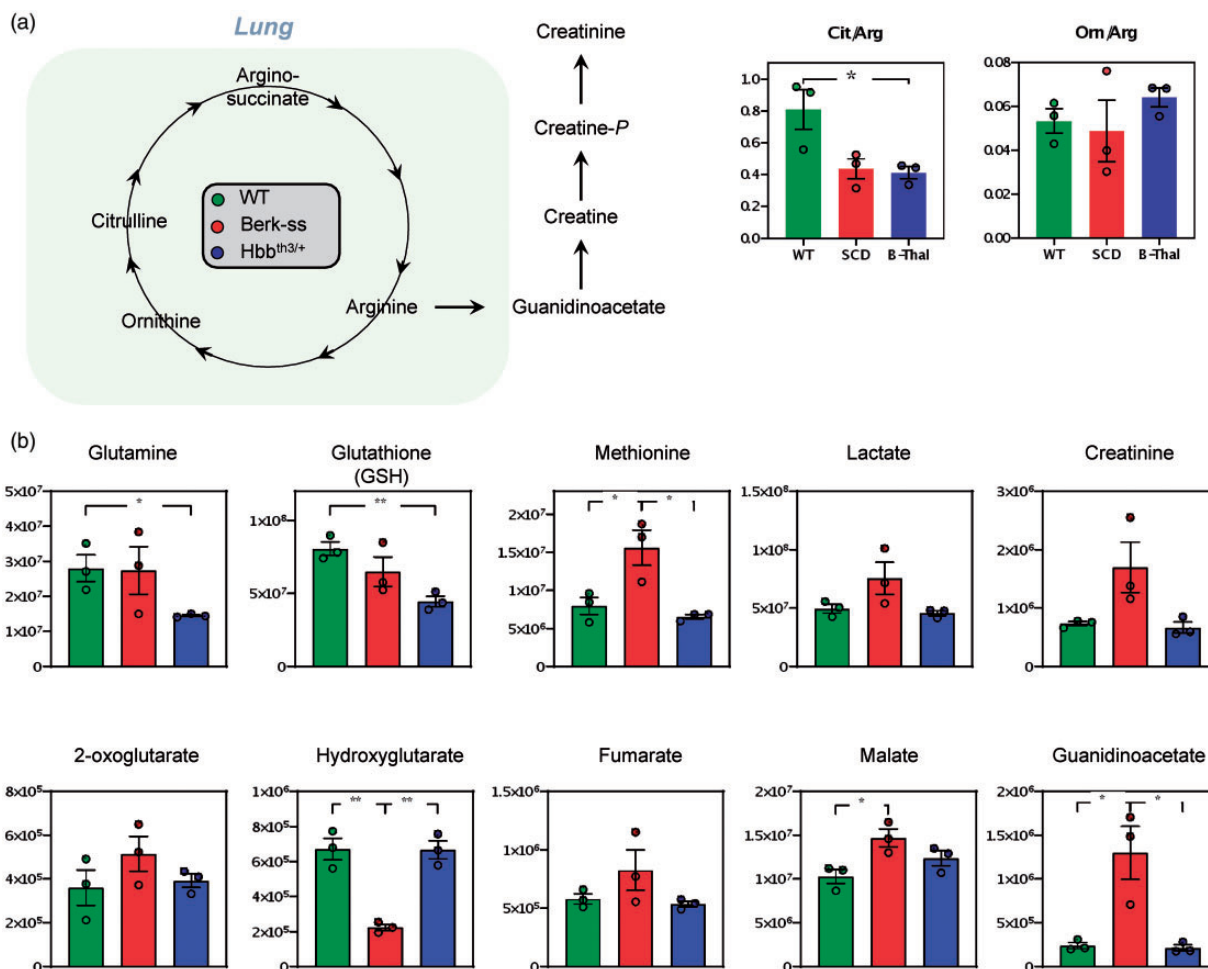
Fig. 5. Lung tissue metabolites that detail primary differences between Berk-ss, Hbb[th3+] and their shared wild type: An overview of arginine metabolism (a) in lungs from wild type (green), sickle cell disease (red), and beta-thalassemia (blue) mice, one of the most affected pathways across the three groups, along with glutaminolysis/glutathione metabolism, methionine metabolism, Krebs cycle, and related carboxylic acids (e.g., 2-hydroxyglutarate – (b)). Asterisks indicate significance by ANOVA (Kruskal-Wallis with Dunn post hoc test; *$p < 0.05$; **$p < 0.01$).

consequence of hemolysis,[11] hypoxia[43,44] and thromboembolic disease.[45] Because there is currently no targeted therapy for hemoglobinopathy associated PH, it is important to identify early proof-of-concept models with the potential for human translational application.

Our previous work identified a unique feature amongst SCA patients suffering from PH, right ventricular failure, and ultimately sudden death that is consistent with high hemoglobin, iron (Fe^{2+} and Fe^{3+}), ferritin heavy chain and lipid peroxidation content macrophages in the adventitia of remodeled pulmonary vasculature.[4] While clinical progression of both β-thalassemia and SCA increase the risk for the development of PH, it remains unclear if common features exist. From a preclinical perspective understanding, the similarities and differences in the cardiopulmonary response of transgenic murine models can aid in development of therapeutics. In the current study, we hypothesized that both Berk-ss and Hbb[th3/+] mice develop pulmonary vascular remodeling, PH, and right ventricular dysfunction. To date, we are unaware of prior studies

comparing cardiopulmonary function in murine models of Group V PH associated with hemolytic hemoglobinopathies.

We report Berk-ss and Hbb[th3/+] mice develop PH with pressures around 30 mmHg, but as high as 40 mmHg. These pressures may also be underestimated due to anesthesia and invasive open chest procedures used with solid state heart catheterization. Regardless, this is consistent with generally stable SCA PH patients who succumb to cardiopulmonary complication with repeated exacerbations of stressors that contribute toward progressive disease.[46] In the absence of external stressors, Berk-ss and Hbb[th3/+] mice develop a similar degree of pulmonary vessel remodeling, cardiac remodeling, and intracellular pulmonary vascular macrophage red blood cell degradation products, resulting in iron accumulation. The potential contribution of macrophage iron represents an intriguing therapeutic target. Studies to date report that iron mitigation strategies may be beneficial in non-transfusion-dependent disease.[4,47–49] Further, overlapping features of human disease such as extracellular
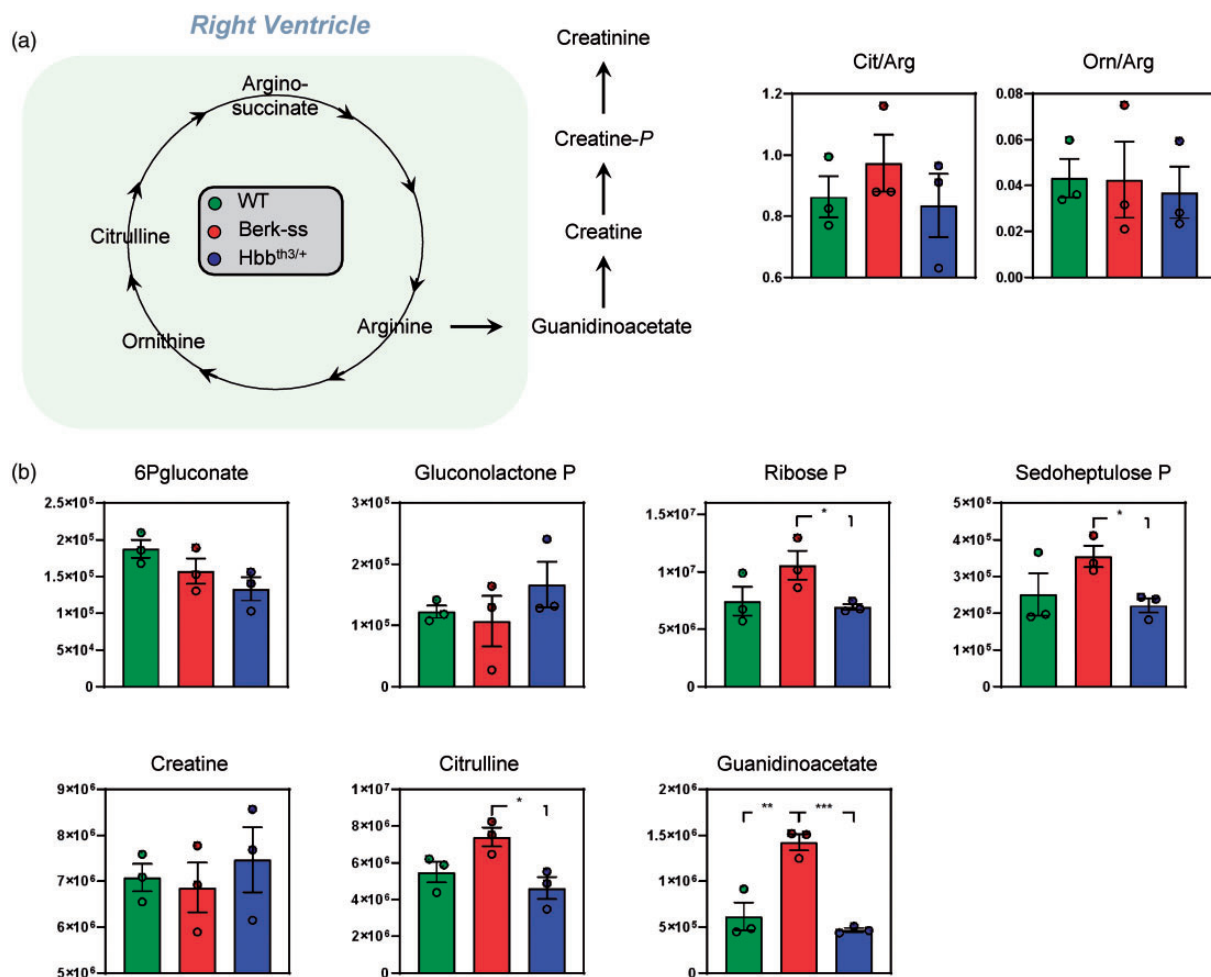
Fig. 6. Right ventricle tissue metabolites that detail primary differences between Berk-ss, Hbb[th/3+] and their shared wild type: An overview of arginine metabolism (a) in the right ventricle (RV) from wild type (green), sickle cell disease (red), and beta-thalassemia (blue) mice, one of the most affected pathways across the three groups, along with the pentose phosphate pathway, glutaminolysis/glutathione metabolism, methionine metabolism, Krebs cycle, and related carboxylic acids (e.g., 2-hydroxyglutarate - b). Asterisks indicate significance by ANOVA (Kruskal-Wallis with Dunn post hoc test; *$p < 0.05$; **$p < 0.01$; ***$p < 0.001$).

Hb accumulation, microparticle accumulation as well as thrombosis remain important targets for therapeutic intervention.

Assessment of right ventricular mechanics provides useful insight into cardiac compensatory responses in the presence of PH. Solid state catheter measurements support PH based similarities in right ventricular afterload in both mice populations; however, right ventricular mechanics support Hbb[th3/+] mice having a restrictive physiology phenotype with preserved contractility, while Berk-ss mice demonstrate impaired RV contraction. Interestingly, neither Berk-ss nor Hbb[th3/+] mice demonstrate changes in right ventricular function (stroke volume, heart rate, or cardiac output), suggesting silent, but significant underlying pathophysiology. Both mice show severe anemia and increased spleen weight, indicative of erythrophagocytosis and extramedullary erythropoiesis in mice. Similar to hypoxic PH, the severe anemic response in these animals likely contributes to the overall process of cardiopulmonary dysfunction,

possibly because of constantly stabilized hypoxia inducible factors (HIF-1 and HIF-2). Neither Berk-ss nor Hbb[th3/+] mice tolerate the anemia, so hyper-erythropoiesis develops with continuous activation of mitogenic factors that may play a role in pulmonary remodeling.[44]

Although there are similarities, WT, Hbb[th3/+], and Berk-ss mice also demonstrate different lung and right ventricular metabolism; Berk-ss mice significantly diverge from WT more than Hbb[th3/+] in the top 25 cardiopulmonary altered metabolites. For example, Hbb[th3/+] mice showed decreased pulmonary glutathione and possible signatures of mitochondrial dysfunction, a hallmark of PH in other rodent, bovine, ovine models, and primary tissue from PH patients.[36,50] On the other hand, right ventricular metabolism in Berk-ss mice showed pentose phosphate pathway activation, the main pathway that contributes reducing equivalents that sustain anabolic demands[51] in proliferating cells, consistent with cellular proliferation in PH[52] and in glucose-6-phosphate dehydrogenase deficiency.[53]

We observe differences in cardiac function and metabolic divergence in the Berk-SS and Hbb$^{th3/+}$ murine models of spontaneous PH. Based on knowledge derived from patient data, PH development is associated with intra-vascular hemolysis, iron accumulation, and microparticle (RBC and endothelial)-induced endothelial dysfunction/thrombosis in both diseases.[13–15,18,54] These contributors to the pathophysiology of PH development likely become more pronounced with age concomitant with a lifetime of exposure to hemolysis, endothelial dysfunction, and anemia in murine models. Molecular contributors that include decreased nitric oxide bioavailability that occurs after Hb consumption and/or arginase elevation, heme/iron-induced oxidative processes, and intermittent bouts of hypoxia that occur with RBC clearance are expected to contribute as underlying mechanisms.[4,55,56] Interestingly, functional and tissue metabolic differences are observed in the two murine models evaluated here.

In summary, the study provides a direct comparison of the pulmonary vascular and right ventricular phenotypes associate with SCA (Berk-ss) and β-thalassemia intermedia (Hbb$^{th3/+}$) mice, two murine models of genetic hemolytic hemoglobinopathy with potential for translation to human Group V PH. Unique to these models is development of cardiopulmonary dysfunction with similar pulmonary vascular remodeling, and pulmonary vascular iron accumulation. Divergence between the two models is readily observed in cardiac remodeling and right ventricular mechanical parameters. Aspects of disease with commonality such as pulmonary iron accumulation, severe anemia, and an inability to undergo anemia tolerance in the face of hypoxia suggest potential areas of overlap for the study of therapeutic intervention.

Conflict of interest

Funding

Authors' contributions

PWB, DS, DIP, MAF, RBW, AD, DCI: study conception and design, animal studies, solid state catheter experiments, immunohistochemistry, macrophage collection, metabolomic analysis, analysis and interpretation of data, drafting the article. KH, RN: interpretation of data, drafting of the article. All authors read and approved the final article.

Guarantor

DCI and PWB.

Ethical approval

ORCID iDs

Paul W. Buehler (iD) https://orcid.org/0000-0003-0687-3008
David C. Irwin (iD) https://orcid.org/0000-0002-1743-8266

Supplemental Material

Supplemental material for this article is available online.

References

1. McCavit TL. Sickle cell disease. *Pediatr Rev* 2012; 33: 195–204; quiz 205–196.
2. Simpson S. Sickle cell disease: a new era. *Lancet Haematol* 2019; 6: e393–e394.
3. Liu Y, Jing F, Yi W, et al. HO-1(hi) patrolling monocytes protect against vaso-occlusion in sickle cell disease. *Blood* 2018; 131: 1600–1610.
4. Redinus K, Baek JH, Yalamanoglu A, et al. An Hb-mediated circulating macrophage contributing to pulmonary vascular remodeling in sickle cell disease. *JCI Insight* 2019; 1–14.
5. Fraidenburg DR and Machado RF. Pulmonary hypertension associated with thalassemia syndromes. *Ann N Y Acad Sci* 2016; 1368: 127–139.
6. Rund D and Rachmilewitz E. Beta-thalassemia. *N Engl J Med* 2005; 353: 1135–1146.
7. Vallelian F, Gelderman-Fuhrmann MP, Schaer CA, et al. Integrative proteome and transcriptome analysis of extramedullary erythropoiesis and its reversal by transferrin treatment in a mouse model of beta-thalassemia. *J Proteome Res* 2015; 14: 1089–1100.
8. Mannu F, Arese P, Cappellini MD, et al. Role of hemichrome binding to erythrocyte membrane in the generation of band-3 alterations in beta-thalassemia intermedia erythrocytes. *Blood* 1995; 86: 2014–2020.
9. Ginzburg Y and Rivella S. Beta-thalassemia: a model for elucidating the dynamic regulation of ineffective erythropoiesis and iron metabolism. *Blood* 2011; 118: 4321–4330.
10. Gladwin MT and Kato GJ. Cardiopulmonary complications of sickle cell disease: role of nitric oxide and hemolytic anemia. *Hematology* 2005; 2005: 51–57.
11. Gladwin MT, Sachdev V, Jison ML, et al. Pulmonary hypertension as a risk factor for death in patients with sickle cell disease. *New Engl J Med* 2004; 350: 886–895.
12. Simonneau G, Montani D, Celermajer DS, et al. Haemodynamic definitions and updated clinical classification of pulmonary hypertension. *Eur Respir J* 2019; 53: 1–13.
13. Taylor JGt, Nolan VG, Mendelsohn L, et al. Chronic hyperhemolysis in sickle cell anemia: association of vascular

complications and mortality with less frequent vasoocclusive pain. *PLoS One* 2008; 3: e2095.

14. Nouraie M, Zhang X, Srisuwananukorn A, et al. Potential contribution of pulmonary thromboembolic disease in pulmonary hypertension in sickle cell disease. *Ann Am Thorac Soc* 2020; 17: 899–901.

15. Kato GJ, Onyekwere OC and Gladwin MT. Pulmonary hypertension in sickle cell disease: relevance to children. *Pediatric Hematology-Oncology* 2007; 24: 159–170.

16. Schwartz JH, Castellucci VF and Kandel ER. Functioning of identified neurons and synapses in abdominal ganglion of aplysia in absence of protein synthesis. *J Neurophysiol* 1971; 34: 939–953.

17. Gordeuk VR, Castro OL and Machado RF. Pathophysiology and treatment of pulmonary hypertension in sickle cell disease. *Blood* 2016; 127: 820–828.

18. Turpin M, Chantalat-Auger C, Parent F, et al. Chronic blood exchange transfusions in the management of pre-capillary pulmonary hypertension complicating sickle cell disease. *Eur Respir J* 2018; 52: 1–14.

19. Derchi G, Galanello R, Bina P, et al. Prevalence and risk factors for pulmonary arterial hypertension in a large group of beta-thalassemia patients using right heart catheterization: a Webthal study. *Circulation* 2014; 129: 338–345.

20. Atichartakarn V, Chuncharunee S, Archararit N, et al. Intravascular hemolysis, vascular endothelial cell activation and thrombophilia in splenectomized patients with hemoglobin E/beta-thalassemia disease. *Acta Haematol* 2014; 132: 100–107.

21. Atichartakarn V, Chuncharunee S, Archararit N, et al. Prevalence and risk factors of pulmonary hypertension in patients with hemoglobin E/beta-thalassemia disease. *Eur J Haematol* 2014; 92: 346–353.

22. Manakeng K, Prasertphol P, Phongpao K, et al. Elevated levels of platelet- and red cell-derived extracellular vesicles in transfusion-dependent beta-thalassemia/HbE patients with pulmonary arterial hypertension. *Ann Hematol* 2019; 98: 281–288.

23. Tuder RM, Stacher E, Robinson J, et al. Pathology of pulmonary hypertension. *Clin Chest Med* 2013; 34: 639–650.

24. Ferguson SK, Redinius K, Yalamanoglu A, et al. Effects of living at moderate altitude on pulmonary vascular function and exercise capacity in mice with sickle cell anaemia. *J Physiol* 2019; 597: 1073–1085.

25. Hsu LL, Champion HC, Campbell-Lee SA, et al. Hemolysis in sickle cell mice causes pulmonary hypertension due to global impairment in nitric oxide bioavailability. *Blood* 2007; 109: 3088–3098.

26. Manci EA, Hillery CA, Bodian CA, et al. Pathology of Berkeley sickle cell mice: similarities and differences with human sickle cell disease. *Blood* 2006; 107: 1651–1658.

27. Gelderman MP, Baek JH, Yalamanoglu A, et al. Reversal of hemochromatosis by apotransferrin in non-transfused and transfused Hbbth3/+ (heterozygous B1/B2 globin gene deletion) mice. *Haematologica* 2015; 100: 611–622.

28. Grundy D. Principles and standards for reporting animal experiments in The Journal of Physiology and Experimental Physiology. *The Journal of Physiology* 2015; 593: 2547–2549.

29. Buehler PW, Baek JH, Lisk C, et al. Free hemolgobin induction of pulmonary vascular disease: evidence for and inflammatory mechanism. *Am J Physiol Lung Cell Mol Physiol* 2012; 303: 312–326.

30. Stacher E, Graham BB, Hunt JM, et al. Modern age pathology of pulmonary arterial hypertension. *Am J Respir Crit Care Med* 2012; 186: 261–272.

31. Catala A, Youssef LA, Reisz JA, et al. Metabolic reprogramming of mouse bone marrow derived macrophages following erythrophagocytosis. *Front Physiol* 2020; 11: 396.

32. Fox BM, Gil HW, Kirkbride-Romeo L, et al. Metabolomics assessment reveals oxidative stress and altered energy production in the heart after ischemic acute kidney injury in mice. *Kidney Int* 2019; 95: 590–610.

33. Graham BB, Kumar R, Mickael C, et al. Vascular adaptation of the right ventricle in experimental pulmonary hypertension. *Am J Respir Cell Mol Biol* 2018; 59: 479–489.

34. Nemkov T, Reisz JA, Gehrke S, et al. High-throughput metabolomics: isocratic and gradient mass spectrometry-based methods. *Methods Mol Biol* 2019; 1978: 13–26.

35. Pang Z, Chong J, Zhou G, et al. MetaboAnalyst 5.0: narrowing the gap between raw spectra and functional insights. *Nucleic Acids Res*. Epub ahead of print 22 May 2021. DOI: 10.1093/nar/gkab382.

36. D'Alessandro A, El Kasmi KC, Plecita-Hlavata L, et al. Hallmarks of pulmonary hypertension: mesenchymal and inflammatory cell metabolic reprogramming. *Antioxid Redox Signal* 2018; 28: 230–250.

37. Zhang H, Wang D, Li M, et al. Metabolic and proliferative state of vascular adventitial fibroblasts in pulmonary hypertension is regulated through a microRNA-124/PTBP1 (polypyrimidine tract binding protein 1)/pyruvate kinase muscle axis. *Circulation* 2017; 136: 2468–2485.

38. Li M, Riddle S, Zhang H, et al. Metabolic reprogramming regulates the proliferative and inflammatory phenotype of adventitial fibroblasts in pulmonary hypertension through the transcriptional corepressor C-terminal binding protein-1. *Circulation* 2016; 134: 1105–1121.

39. Li M, Riddle S, Kumar S, et al. Microenvironmental regulation of macrophage transcriptomic and metabolomic profiles in pulmonary hypertension. *Front Immunol* 2021; 12: 640718.

40. Hernandez-Saavedra D, Sanders L, Freeman S, et al. Stable isotope metabolomics of pulmonary artery smooth muscle and endothelial cells in pulmonary hypertension and with TGF-beta treatment. *Sci Rep* 2020; 10: 413.

41. Kitagawa A, Kizub I, Jacob C, et al. CRISPR-mediated single nucleotide polymorphism modeling in rats reveals insight into reduced cardiovascular risk associated with Mediterranean G6PD variant. *Hypertension* 2020; 76: 523–532.

42. Machado RF and Gladwin MT. Pulmonary hypertension in hemolytic disorders: pulmonary vascular disease: the global perspective. *Chest* 2010; 137: 30S–38S.

43. Sachdev V, Kato GJ, Gibbs JS, et al. Echocardiographic markers of elevated pulmonary pressure and left ventricular diastolic dysfunction are associated with exercise intolerance in adults and adolescents with homozygous sickle cell anemia in the United States and United Kingdom. *Circulation* 2011; 124: 1452–1460.

44. Zhang X, Zhang W, Ma SF, et al. Hypoxic response contributes to altered gene expression and precapillary pulmonary hypertension in patients with sickle cell disease. *Circulation* 2014; 129: 1650–1658.

45. Lim MY, Ataga KI and Key NS. Hemostatic abnormalities in sickle cell disease. *Curr Opin Hematol* 2013; 20: 472–477.

46. D'Alonzo GE, Barst RJ, Ayres SM, et al. Survival in patients with primary pulmonary hypertension. Results from a national prospective registry. *Ann Intern Med* 1991; 115: 343–349.

47. Li H, Rybicki AC, Suzuka SM, et al. Transferrin therapy ameliorates disease in beta-thalassemic mice. *Nat Med* 2010; 16: 177–182.

48. Low PS. Infantile spasms – a clinical perspective. *J Singapore Paediatr Soc* 1989; 31: 147–152.

49. Manolova V, Nyffenegger N, Flace A, et al. Oral ferroportin inhibitor ameliorates ineffective erythropoiesis in a model of beta-thalassemia. *J Clin Invest* 2019; 130: 491–506.

50. Plecita-Hlavata L, Tauber J, Li M, et al. Constitutive reprogramming of fibroblast mitochondrial metabolism in pulmonary hypertension. *Am J Respir Cell Mol Biol* 2016; 55: 47–57.

51. Fan J, Ye J, Kamphorst JJ, et al. Quantitative flux analysis reveals folate-dependent NADPH production. *Nature* 2014; 510: 298–302.

52. Joshi SR, Kitagawa A, Jacob C, et al. Hypoxic activation of glucose-6-phosphate dehydrogenase controls the expression of genes involved in the pathogenesis of pulmonary hypertension through the regulation of DNA methylation. *Am J Physiol Lung Cell Mol Physiol* 2020; 318: L773–L786.

53. Varghese MV, James J, Rafikova O, et al. Glucose-6-phosphate dehydrogenase deficiency contributes to metabolic abnormality and pulmonary hypertension. *Am J Physiol Lung Cell Mol Physiol* 2021; 320: L508–L521.

54. Saraf SL, Zhang X, Kanias T, et al. Haemoglobinuria is associated with chronic kidney disease and its progression in patients with sickle cell anaemia. *Br J Haematol* 2014; 164: 729–739.

55. Morris CR, Kato GJ, Poljakovic M, et al. Dysregulated arginine metabolism, hemolysis-associated pulmonary hypertension, and mortality in sickle cell disease. *JAMA* 2005; 294: 81–90.

56. Reiter CD, Wang X, Tanus-Santos JE, et al. Cell-free hemolgobin limits nitric oxide bioavailability in sickle-cell disease. *Nat Med* 2002; 8: 1383–1389.